Crystal structures and spin crossover in the polymeric material [Fe(Htrz)2(trz)](BF4) including coherent-domain size reduction effects

Arnaud Grosjean, Philippe Négrier, Pierre Bordet, Céline Etrillard, Denise Mondieig, Stanislav Péchev, Eric Lebraud, Jean-François Létard, Philippe Guionneau

Crystal Structures and Spin Crossover in the Polymeric Material $[Fe(Htrz)_2(trz)](BF_4)$ Including Coherent-Domain Size Reduction Effects

Arnaud Grosjean,[a] Philippe Négrier,[b] Pierre Bordet,[c] Céline Etrillard,[a] Denise Mondieig,[b] Stanislav Pechev,[a] Eric Lebraud,[a] Jean-François Létard,[a] and Philippe Guionneau*[a]

Keywords: Spin crossover / Powder X-ray diffraction / Phase transitions / Polymers / Iron

The high-spin and low-spin crystal structures of $[Fe(Htrz)_2(trz)](BF_4)$ (Htrz = 1*H*-1,2,4-triazole, trz^- = deprotonated triazolato ligand) were determined and refined on the basis of X-ray diffraction data obtained from a high-quality crystalline powder. Noteworthy differences to the previously reported structural hypothesis are obtained, which includes a revision of the space group to orthorhombic *Pnma*. Notably, the distinction between the positions of the Htrz and the trz^- ligand along the chains reveals their respective roles in the formation of direct interchain interactions. The latter are also mediated by the anions. In addition, the pair-distribution-function (PDF) method was applied to investigate the potential modification of the crystal structure by a reduction of the coherent-domain size from 50 nm to 10 nm. First, the PDF investigation confirms the validity of the crystal structures presented here. Furthermore, in a first approach, it reveals that the crystal structure description remains suitable for the whole range of coherent-domain sizes investigated.

Introduction

Among the spin-crossover (SCO) materials, the triazole-based polymeric compound of the formula $[Fe(Htrz)_2(trz)](BF_4)$ attracts special attention (Htrz = 1*H*-1,2,4-triazole, trz^- = deprotonated triazolato ligand).[1] Indeed, it was very early depicted as one of the most promising SCO materials for memory devices,[2] and it is still cited nowadays as the ideal system for technological applications.[3] The initial interest was undoubtedly due to the exceptional properties of this compound, which shows SCO slightly above room temperature with a large hysteresis (ca. 40 K) and an attractive reversible white-to-pink color change associated to the transition from a high-spin (HS) to a low-spin (LS) state. In addition, this compound is strongly involved in the race to the design of nano-sized polymeric SCO materials.[4,5] Recently, it was also used to discover novel routes towards the synergy between electrical and SCO properties.[6,7] In parallel, curiously, few is known about some fundamental aspects of this compound, which includes the structural properties. It is well-known and was demonstrated for molecular SCO materials that the structural properties are closely related to the SCO features and vice versa.[8] Therefore, the current lack of structural data represents a strong restraint to the further development and the understanding of the SCO properties of $[Fe(Htrz)_2(trz)](BF_4)$. This lack mainly stems from the fact that no single crystals were obtained so far, despite decades of trials. Interestingly, until very recently, the same difficulty, due to a lack of structural data affected the whole family of polymeric, triazole-based SCO materials of the general formula $[Fe(R\text{-}trz)_3]X_2$ (R-trz = triazole derivative), to which the title compound is related to some extend. The first single crystals have just been obtained for $R = NH_2$ with $X = NO_3^-$[9] and $X = BF_4^-$,[10] which allows the first descriptions of the structural properties of the polymeric $[Fe(R\text{-}trz)_3]X_2$ SCO family and gives hope for a systematic structural investigation of this SCO family. Nevertheless, this is not yet the case for $[Fe(Htrz)_2(trz)](BF_4)$, for which only badly crystallized powders were investigated so far. Furthermore, it is even known that large crystalline particles cannot be obtained for this compound, because the synthesis leads to a maximum particle size of a few hundred nm.[11] The formation of powders, which show only poor diffraction patterns, is indeed the second reason for the lack of reliable structural data. As a consequence, the sole structural data used for this compound during the last decades came from X-ray absorption techniques.[12] These data only give a structural description of the close proximity of the metal centers and were used to corroborate the 1D polymeric structure, but

[a] CNRS, Univ. Bordeaux, ICMCB, UPR 9048,
87 avenue du Dr A. Schweitzer, 33608 Pessac, France
E-mail: guionneau@icmcb-bordeaux.cnrs.fr
Homepage: http://www.icmcb-bordeaux.cnrs.fr/
[b] Univ. Bordeaux, LOMA, UMR 5798,
33400 Talence, France
[c] Institut Néel, CNRS-UJF,
Grenoble, France

they gave no information on the crystal structure itself. Recently, a powder X-ray diffraction (PXRD) study on $[Fe(Htrz)_2(trz)](BF_4)$ led to a first structural hypothesis for both the HS and the LS species.[13] However, the PXRD diffractogram was of very low quality, which was probably due to too small coherent domains (a few nm), which resulted in very large Bragg peaks. Thus, the structural description appeared limited and even questionable. The present work presents a re-determination of the crystal structures of $[Fe(Htrz)_2(trz)](BF_4)$ on the basis of PXRD data from crystalline powder sample with a coherent-domain size as large as it can be obtained for this compound so far (ca. 50 nm). In a second part, the pair distribution function (PDF)[14] was used to investigate the structural properties as a function of the coherent-domain size of the particles, which ranged from 10 to 50 nm. It is worth noting that we preferentially refer in this paper to the coherent-domain size and not to the particle size, because the diffraction properties are related to the former. It is obvious that the coherent-domain size is smaller than the particle size. The relation between the coherent-domain size and particle sizes in $[Fe(R\text{-}trz)_3]X_2$ materials was discussed elsewhere, and the particle size decreases with the coherent-domain size.[15]

Results and Discussion

1. SCO and Crystal Structures

a. Crystal Structure Determination

The crystal structures of $[Fe(Htrz)_2(trz)](BF_4)$ were determined and refined at 420 K, when the sample is white and in the HS state, and at room temperature (300 K), when the sample is pink and in the LS state. Both structures were determined from a crystalline powder optimized for this purpose, which necessitated numerous trials to select the best diffracting powder. Obviously, it was checked that all crystalline powders from this compound present identical diffraction patterns, that is, they correspond to the same crystal structure. The investigated sample consists of particles that look like plates with a few hundred nm of length, the thickness of which could not be determined, because each visible grain is in fact a stack of numerous plates. The calculation of the corresponding average coherent-domain size[15] gives a value of approximately 50 nm (i.e., 500 Å). The resulting X-ray diffraction patterns are of relatively good quality (Figure 1) and the crystal structure determination and refinement appear reliable (Table 1).

The pattern matching and the crystal structure refinement parameters appear better than those obtained for the previously reported crystal structure of this sample.[13] The reason for such a discrepancy is probably the bad quality of the PXRD pattern used by the authors, which showed very broad Bragg peaks because of a very small coherent-domain size. One of the crucial differences concerns the space group, because the sample in fact crystallizes in *Pnma* and not in *Cmcm* as previously reported. The latter space group does not allow taking into account all Bragg peaks actually observed in the present pattern. Furthermore, the quality of the present results allows a description of the crystal packing and, notably, makes it possible to distinguish between Htrz and trz^- positions within the chains. We thus assume that this re-investigation of the crystal structure allows for a consistent structural description, and the present results are used below to comment on the structure–properties relationship of the title compound.

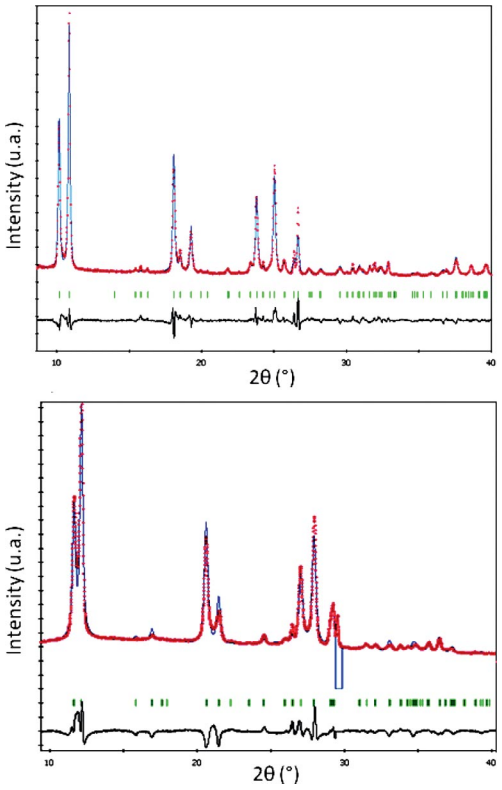

Figure 1. Experimental (red circles) and calculated (blue line) diffraction patterns and the difference profile (black line) of $[Fe(Htrz)_2(trz)](BF_4)$ in the LS state at room temperature (top) and in the HS state at 420 K (bottom). The excluded region is due to the alumina oxide support.

Table 1. Crystal unit cell and results of the Rietveld refinement for $[Fe(Htrz)_2(trz)](BF_4)$ in the LS and HS state. See experimental section for methodology details.

	Low spin	High spin
Temperature [K]	300	420
Crystal system	orthorhombic	orthorhombic
Space group	*Pnma*	*Pnma*
a [Å]	17.3474(16)	17.4968(17)
b [Å]	7.3247(6)	7.7874(9)
c [Å]	9.1907(9)	9.5643(9)
Volume [Å^3]	1167.8(2)	1303.2(2)
Wavelength, $K_\alpha 1$ [Å]	1.540562	1.789000
2θ angular range [°]	8.0–40.0	8.0–60.0
R_{wp} [%]	10.23	4.69
R_p [%]	7.58	3.25
Overall isotropic temp. factor *U* [Å^2]	0.052(2)	0.126(3)

b. Crystal Structure Description

The crystal structure is based on an asymmetric unit, which contains ½ $[Fe(Htrz)_2(trz)](BF_4)$, because Htrz, trz^-, and BF_4 lie on a mirror plane, and the iron center lies on an inversion center. The triazole ligands are connected to the iron center. The symmetry operations lead to the alignment of the Fe^{II} centers along the *b* axis with the three bridging triazoles in alternating invert positions (Figure 2). The relation between the unit-cell parameters and the positions in the $[Fe(Htrz)_2(trz)]_n$ chain is shown on Figure 2. By symmetry, all the chains within the crystal packing are identical. Within the $[Fe(R\text{-}trz)_3]X_2$ family, one of the peculiar aspects of the title compound is the subtly nonsymmetrical environment of the metal center, because the latter is connected to two Htrz ligands and one trz^- ligand, which gives the charged formula $[Fe^{II}(Htrz)_2(trz^-)](BF_4^-)$. Furthermore, a novel aspect shown by the present result is that by taking into account the *Pnma* crystal symmetry we can distinguish between the Htrz and trz^- ligands within the chains (Figure 2), which allows to determine their individual function within the crystal packing (see Figures 3 and 4). Another interesting point of the present work is that the position of the BF_4^- anion could be refined, which allows a reliable positioning within the crystal structure. Each BF_4^- ion is located in cavities formed by the triazole ligands (Figure 5). Furthermore, it is worth noting that no water molecule was found within the crystal structure and that there is no void left that could fit a water molecule.

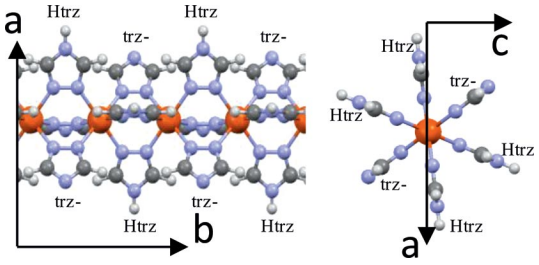

Figure 2. View of a segment of the $[Fe(Htrz)_2(trz)]_n$ chain (left) along *c* and (right) along *b*. Both views underline the specific positions of Htrz and trz^-. Blue: nitrogen; orange: iron; dark-grey: carbon; light-grey: hydrogen.

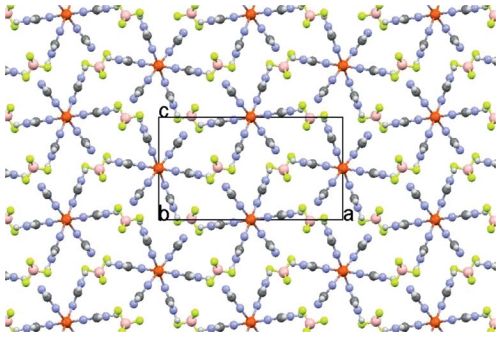

Figure 3. View along the *b* axis of the crystal packing of $[Fe(Htrz)_2(trz)](BF_4)$.

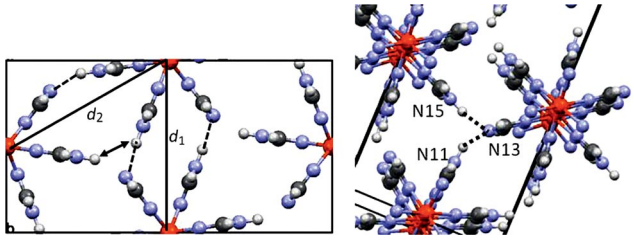

Figure 4. Details of the crystal packing with a focus on interchain distances in $[Fe(Htrz)_2(trz)](BF_4)$, shows (left) the Fe–Fe interchains distances d_1 and d_2 along with the hydrogen bond (dotted lines) and repulsed H atoms (arrow) and (right) the Htrz–trz^- interactions. (see Table 2).

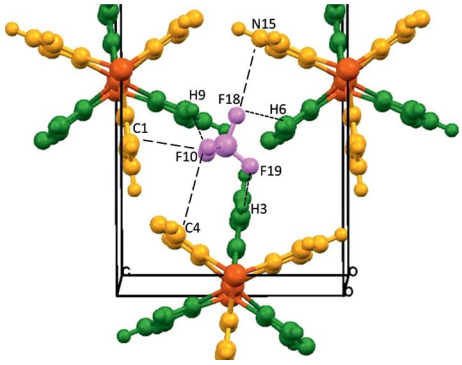

Figure 5. View of the BF_4^--anion cavities within the crystal packing of $[Fe(Htrz)_2(trz)](BF_4)$ with the triazole ligands in the same mirror plane (yellow) as the anion and the ones in the plane below the anion (dark green). The shortest distances between the anion and the chains are visualized. See Table 3 for distances.

The distance between two neighboring iron centers within a chain is exactly half of the *b* parameter. Consequently, in this compound, the measurement of the unit cell allows to determine the intrachain Fe–(N=N)–Fe distance, which is directly related to the SCO, because Fe–N dis-

Table 2. Distances and angles corresponding to the direct interchain interactions between the Htrz and trz^- ligands (see Figure 4 for labels).

		N–H···N Bond angles [°]	N–H···N Bond lengths [Å]	N···N distances [Å]
N15–H···N13	LS	175.97	1.9099(2)	2.9062(3)
	HS	169.95	1.9174(2)	2.9056(3)
N11–H···N13	LS	158.03	1.8930(1)	2.8430(2)
	HS	151.89	1.8030(1)	2.7244(2)

Table 3. Selected shortest distances [Å] between the chains and BF_4^- in the HS and LS structures of $[Fe(Htrz)_2(trz)](BF_4)$. See Figure 5 for labels.

Interaction	Ligand	Atoms	LS	HS
F···H–C	Htrz	F10···H9	2.4331(2)	2.1056(2)
	Htrz	F19···H3	2.4019(1)	2.3740(2)
	trz^-	F18···H6	2.5110(2)	2.6720(2)
F···N	Htrz	F18···N15	3.2975(3)	3.4400(3)
F···C	Htrz	F10···C1	3.3835(3)	3.3162(3)
	trz^-	F10···C4	3.7398(3)	3.9280(3)

tances are known to vary by about 0.2 Å from HS to LS state.[8] Here, the SCO corresponds to a change of the intrachain Fe–Fe distance of 0.23 Å, because *b* varies between 3.8937(5) Å (HS) and 3.6624(3) Å (LS). The relative variance of *b* caused by the SCO (ca. 6.3%) is the strongest variation within the unit cell (ca. 1.0% for *a* and ca. 4.0% for *c*). Thus, the unit-cell variation connected to the SCO emphasizes that all dimensions of the crystal are affected, although the effect is much more pronounced for the chain length. The corresponding volume variation (11.5%) appears larger than in other SCO materials (1–5%).[8] The unit-cell variations found here are in line with those previously found for this sample.[13]

Each $[Fe(Htrz)_2(trz)]_n$ chain is surrounded by six identical adjacent chains (Figure 3) with two different Fe–Fe interchain distances denoted d_1 and d_2 (Figure 4). d_1 is the distance between one chain and the two closest neighboring chains, and it matches with *c*, whereas d_2 corresponds to the distance to the four other chains. Accordingly, d_2 is significantly larger (9.816 Å in the LS and 9.970 Å in the HS state) than d_1 (9.191 Å in the LS and 9.564 Å in the HS state). The crystal packing shows a pseudohexagonal structure, and it is the difference between d_1 and d_2 that mainly prevents $[Fe(Htrz)_2(trz)](BF_4)$ to adopt a hexagonal unit cell. The discrepancy between d_1 and d_2 can be easily explained by considering the relative positions of the Htrz and trz^- ligands (Figure 4). Indeed, in the interchain direction, which corresponds to d_1, Htrz alternates with trz^-, whereas in the direction corresponding to d_2 Htrz also faces Htrz, not only trz^-, which leading to repulsion between hydrogen atoms. As a result, d_2 is longer than d_1. Hence, the deviation from the hexagonal description originates from the distinction between the Htrz and trz^- positions. This result may explain why pseudohexagonal solutions are sometimes obtained when poor-quality diffractograms of $[Fe(Htrz)_2(trz)](BF_4)$ are indexed.

The relative vicinity of the chains and the density of the crystal packing lead to interchain interactions, the presence of which has always been a controversially discussed topic. Here, it is proven that the chains are directly linked through N–H···N interactions involving Htrz and trz^- ligands (Figure 4, Table 2). The Htrz ligands are clearly pointing in the direction of the trz^- molecules. The very short N···N and N–H···N distances evidence a relatively strong network of interchain interactions. One of these N–H···N distances appears to shorten upon the transition from LS to HS, which results in an expansion of the Fe–N distances and possibly leads to a stronger interaction in the HS state.

In addition, the BF_4^- anions also contribute to the cohesion of the crystal packing (Figure 5). Relatively short distances between the F atoms and the triazole ligands are evidence for anion–chain interactions (Table 3). Within the crystal packing, the BF_4^- ion is surrounded by twelve triazole ligands, six of which are in the mirror plane that also contains the B atom, and the other six of which are on both sides of this mirror plane (Figure 5). The shortest distances are those to the latter six, which highlights the fact that the anion–chain interactions occur mainly along the *b* axis. The anion interacts with all neighboring chains, which, to some extend, may be seen as indirect interchain interactions mediated by the anion. The distances between BF_4^- and trz^- are longer than those between BF_4^- and Htrz, which shows that the anions are repulsed by the charge of trz^-. Upon going from LS to HS, all the anion···trz^- distances increase, whereas the pattern is more intricate for the anion···Htrz distances, some of which shorten (Table 3). This behavior simply reflects the tendency of BF_4^- to move away from trz^-. Indeed, the volume of the BF_4^- cavity is larger in the HS state than it is in the LS state, and the anion adjusts its position to increase the distances to the trz^- ligands.

The well-known strong cooperativity and the large hysteresis shown by $[Fe(Htrz)_2(trz)](BF_4)$ were often ascribed to the presence of water molecules linking the chains. This work reveals that there is no water inside the structure. The cooperativity originates from short interchain contacts, which are basically of two types: direct interactions through Htrz–trz^- contacts and indirect interactions through chain–BF_4^-–chain interactions.

2. PDF Analysis and Coherent-Domain Size

Nowadays, the size reduction of samples, for example, to nano-sized particles, is one of the focus topics in material sciences. The field of SCO research does not escape this trend, because the preparation of SCO nanoparticles is of prime interest. In particular, the $[Fe(R\text{-}trz)_3]X_2$ family and $[Fe(Htrz)_2(trz)](BF_4)$ are the focus of many efforts.[3,5,6,8,15] In this context, one of the questions that may be raised concerns the validity of a structural description that is based on classical XRD data of micro or macrosamples but is supposed to describe nano-sized samples. To illustrate this point, we present in Figure 6 the crystal packing of $[Fe(Htrz)_2(trz)](BF_4)$, as it would appear in a 10 nm or a 2 nm coherent domain, if the crystal structure presented above was still the same at these scales. Let us recall, that we used a powder with a coherent-domain size of 50 nm to determine the crystal structure. This figure illustrates the number of chains or metallic centers involved at such sizes.

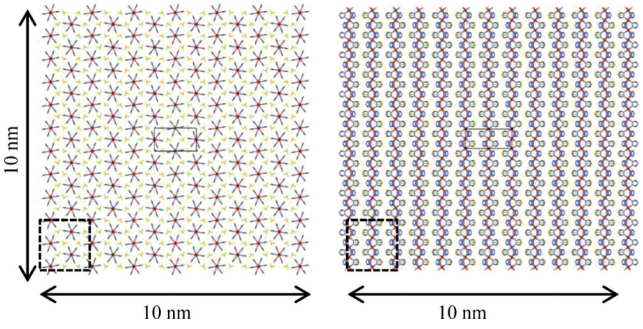

Figure 6. Representation of the crystal packing inside a virtual, cubic coherent domain with a side length of 10 nm; views along *b* (left) and along *c* (right). The dashed line in the lower left part of each figure encloses a 2 nm square.

A reduction of the coherent-domain sizes to a few nm prevents the use of classical X-ray diffraction to investigate the crystal structures of the samples. Consequently, to see if this structural description remains correct for the smallest coherent-domain sizes, we used the pair-distribution-function (PDF) approach. It allows to get local structural information even for real nanoparticles.[14] This method is based on the measurement of total-scattering data from high-quality PXRD experiments, and it yields the probability of finding a pair of atoms at a given distance from each other within a sample irrespective of its ordering degree. It is then possible to refine against the observed PDF a structural model in direct space in a similar way the Rietveld refinement is used in reciprocal space for crystalline materials. We first used the PDF analysis method to check the validity of the *Pnma* structural model by refining the PDF up to 30 Å. The fit obtained is shown in Figure 7.

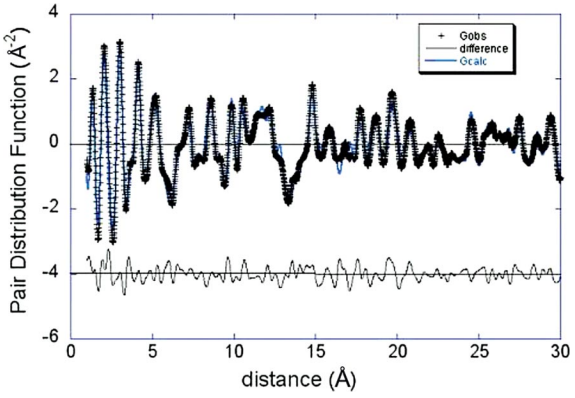

Figure 7. Refinement of the PDF for $[Fe(Htrz)_2(trz)](BF_4)$ up to 30 Å for the *Pnma* crystal structure determined in this work.

This refinement gives a rather satisfactory result with R_w = 24.5% and an average distance of approximately 0.2 Å with the Rietveld-refined structure. Note that the refinement with the atomic positions fixed to the Rietveld values already leads to a reasonable result with R_w = 34.3%, whereas attempts to refine the PDF with the structure proposed by Urakawa et al. lead to a R_w value close to 80% under the same conditions with considerable discrepancies between observed and calculated PDFs. These results validate the crystal structure determination presented in this work.

The atomic-pair distances must be identical if the investigated samples have the same crystal structure. Consequently, by comparing the PDF of different samples, one can easily detect obvious structural differences between them. We thus compared the PDF of three powders of $[Fe(Htrz)_2(trz)](BF_4)$ of different particles size (i.e., ca. 185 × 700 nm, ca. 40 × 40 nm, and ca. 20 × 40 nm. The corresponding coherent-domain sizes were calculated from the PXRD patterns at values of approximately 50, 20, and 10 nm, respectively. Interestingly, this result suggests that the reduction of the particle size concomitantly influences the coherent-domain size, as already found for materials of the same family.[15] The experimental PDFs calculated for distances up to 50 Å are presented in Figure 8 for the three samples.

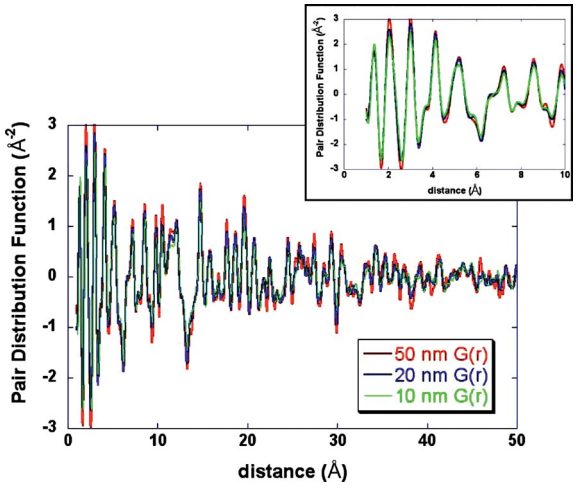

Figure 8. PDF of $[Fe(Htrz)_2(trz)](BF_4)$ at 300 K for different domain sizes, calculated for atomic pair distances up to 50 Å. A closer view for distances up to 10 Å is shown in the inset.

The good superposition of the curves indicates that, as a first approximation, the crystal structure is not significantly affected by the size reduction from 50 to 10 nm. This is true in particular for short distances (<10 Å). For long distances, the three PDFs are also rather similar, small differences are seen for distances bigger than 30 Å, but this may be due to the vicinity of the end of the XRD signal for the 10 nm sample. The refinement of the PDF for the three samples leads to very similar results, and the main difference is the refined value of the average coherent-domain diameter. For all samples, the diameters are smaller than expected and smaller than those found above for the PXRD patterns. This discrepancy may be due to an inhomogeneous distribution of domain sizes and due to the fact that a spherical model is used in the PDF calculation, whereas the domains are expected to be very anisotropic. Nevertheless, these PDF refinements indicate that the global crystal-structure description given in the present work, which includes intrachain and chain-to-chain interactions, still appears to be valid when the coherent-domain size is reduced – at least down to 10 nm. However, it is clear that more precise PDF investigations, for example, with synchrotron sources, are required to get a deeper insight into possible small structural modifications caused by sample size reduction. Such investigations could also provide a reliable description of the coherent-domain size and shape.

Conclusions

The crystal structures of $[Fe(Htrz)_2(trz)](BF_4)$ in the HS and the LS state were determined. Notably, thanks to the discrimination between the relative positions of Htrz and

trz^-, a detailed description of the chains and of the crystal packing could be given. The SCO strongly affects the volume of the unit cell mainly along the chain axis, but the overall structural description remains the same in the HS and the LS state. Nevertheless, together with the intrachain Fe–Fe distances, the SCO also affects interchain contacts, principally those involving the anion. Firstly, this structural study confirms the chain architecture, that is, the polymeric character, of the sample, and secondly, it reveals that the $[Fe(Htrz)_2(trz)]_n$ chains are connected through short N–H···N contacts. This feature, as well as all the structural properties discussed here, should be taken into account to understand the SCO properties of the related family of compounds, especially, because the PDF investigation conducted in this work showed that, as a first approximation, the crystal structure is not affected by a reduction of the coherent-domain size from approximately 50 to approximately 10 nm.

Experimental Section

Synthesis of Crystalline Powders: The samples were obtained by using the reverse-micelle technique already published.[11] Particles with sizes of 185×700 nm, which were used for the crystal structure determination, were first prepared by mixing two solutions, one of an iron(II) salt $Fe(BF_4)_2$ (2 mmol) in demineralised water (1.6 mL) with a trace amount of ascorbic acid and one of the triazole in demineralised water (1.6 mL). The reverse micelles were then obtained by mixing each of those two solutions with the tergitol NP-9 (from the Nonylphenol Ethoxylate family), which played both the role of surfactant and organic solvent (the water–surfactant mass ratio was 75%). The two resulting solutions were then heated to 80 °C for 15 min and subsequently mixed for one hour. The compound was then extracted from the surfactant by using diethyl ether and washed several times. Particles with sizes of 40×40 nm, which were used for the PDF experiment, were obtained by following the same protocol and varying the concentration of $Fe(BF_4)_2$ (6 mmol). Particles with sizes of 20×40 nm were obtained by replacing the tergitol NP-9 with Lauropal (Ifralan D0205, a member of the polyoxyethylenic family), which also plays the role of surfactant and oil (the surfactant–water mass ratio was 75%).[16]

X-ray Powder Diffraction: The data for the LS state at room temperature were recorded by using a PANalytical X'Pert Pro diffractometer [Cu-$K_{\alpha 1}$, Ge (111) monochromator, X'Celerator detector] within the range 8–40° (2θ) by using a scan speed of 3.58° per hour. The data for the HS state at 420 K were recorded by using a PANalytical X'Pert Pro diffractometer (Co-K_α, Fe β-filter, X'Celerator detector) within the range 8–60° (2θ) by using a scan speed of 1.22° per hour. The use of an Anton Paar HTK1200 oven to heat the sample generated peaks in the diffraction pattern that originate from the aluminum oxide support, which were then excluded.

Crystal Structure Determination and Refinement Methodology: Peak positions were determined manually by using the peak-picking option of the PC modeling platform Materials Studio.[17] Potential solutions of cell parameters and space groups were obtained by using the X-Cell algorithm.[18] The cell parameters and the space group that best reproduced the experimental diffraction patterns were chosen and refined by using a Pawley profile-fitting procedure.[19] A Pawley refinement was used to provide refined cell parameters, the peak-profile parameters (profile function, full width at half maximum), the background shift, and the zero shift. Some bond lengths and angles were constraints during the refinement on the basis of CSD values. The BF_4^- ions were set at values of 1.363 Å and 109.47° for the B–F distance and the F–B–F angle, respectively. The bond lengths and angles of Htrz were set at 1.3787, 1.325, and 1.3496 Å and 105.1, 114.85, and 100.1° for the bonds N–N, N–C (N atom linked to the Fe center), and C–N and the angles N–N–C, N–C–N, and C–N–C, respectively. The BF_4^- ion was then set as a rigid body with the mirror restraint from the space group. The Htrz ligand was then linked to the Fe atoms with an Fe–N bond length set to 1.977 Å for the LS state and 2.192 Å for the HS state (considering standard values from the Cambridge Structural Database) and an angle between the coplanar Htrz rings set at 120°. The final drawn monomeric $[Fe(Htrz)_3]^{2+}$ was then set as a rigid body. The drawn molecules were placed inside the unit cell according to the previous structural resolution and matching the mirror planes (BF_4^- and Htrz) and inversion centers (Fe) from the *Pnma* space group. The total number of degrees of freedom is four: Two translations along the *a* and *c* axes for BF_4^- and two rotations around *b* for BF_4^- and $[Fe(Htrz)_3]^{2+}$. The following Rietveld procedure included the refinement of the translation, the rotation of the molecules, the global isotropic temperature factors, and the preferred orientations, and it also included the parameters previously refined in the Pawley procedure. Preferred-orientation corrections of the powder sample were made by using the Rietveld–Toraya function.[20,21] For the first refinement, all triazoles were treated as Htrz ligands. Then, for all the remaining refinement steps, one out of the three triazoles was changed to a trz^- ligand, and the triazoles that were changed were selected on the basis of evident symmetry considerations with respect to the crystal packing. The experimental and the final calculated profiles for the compound are shown in Figure 1. The calculated and experimental profiles are in good agreement, as shown by the difference plot and the reliability parameters (Table 1) that validate the methodology employed.

CCDC-900726 (for the LS state) and -900727 (for the HS state) contain the supplementary crystallographic data for this paper. These data can be obtained free of charge from The Cambridge Crystallographic Data Centre via www.ccdc.cam.ac.uk/data_request/cif.

Pair-Distribution-Function Experiment and Methodology: The data for the three nanoscale samples (coherent-domain sizes of 50, 20, and 10 nm) were recorded with a Bruker–Nonius *k*-CCD diffractometer equipped with an Incoatec IμS AgK_α micro-source X-ray generator and an AppexII-CCD camera detector. Samples were contained in a 0.3 mm diameter borosilicate glass capillary. 36 images were recorded every 3°(2θ) from 2θ = 0°. The diffraction images were then integrated and averaged to yield and complete I(2θ) diffraction pattern up to 2θ = 120°. The PDFs were then obtained and modeled by using the PDFGetX2[22] and PDFGui software.[23] The data up to Q = 18 $Å^{-1}$ were corrected for signals not belonging to the sample, for absorption, and for inelastic or incoherent scattering. The data were then normalized and Fourier transformed to yield the pair distribution function. For the PDF refining of the $[Fe(Htrz)_2(trz)](BF_4)$ structure, the only positional constraints for non-H atomic positions were those imposed by the space group symmetry. H atoms were kept fixed. Three isotropic atomic displacement parameters were refined with constraints to equality for (1) C, N, and H, (2) B and F, and (3) Fe atomic species. The average diameter of the coherent domain was refined by using a spherically shaped model.

Acknowledgments

Support from the Aquitaine Region (PhD grant to A. G.) is gratefully acknowledged.

[1] J. Kröber, J. P. Audière, R. Claude, E. Codjovi, O. Kahn, J. G. Haasnoot, F. Grolière, C. Jay, A. Bousseksou, J. Linarès, F. Varret, A. Gonthier-Vassal, *Chem. Mater.* **1994**, *6*, 1404–1412.

[2] O. Kahn, C. J. Martinez, *Science* **1998**, *279*, 44–48.

[3] G. Aromi, L. A. Barros, O. Roubeau, P. Gamez, *Coord. Chem. Rev.* **2011**, *255*, 485–546.

[4] J. F. Létard, P. Guionneau, L. Goux-Capes, *Top. Curr. Chem.* **2004**, *235*, 221; J. F. Létard, N. Daro, O. Nguyen, WO 2007/065996, **2007**; E. Coronado, J. R. Galán-Mascarós, M. Monrabal-Capilla, J. García-Martínez, P. Pardo-Ibánez, *Adv. Mater.* **2007**, *19*, 1359; J. Larionova, L. Salmon, Y. Guari, A. Tokarev, K. Molvinger, G. Molnár, A. Bousseksou, *Angew. Chem.* **2008**, *120*, 8360; A. Bousseksou, G. Molnár, L. Salmon, W. Nicolazzi, *Chem. Soc. Rev.* **2011**, *40*, 3313.

[5] D. Mader, S. Pillet, C. Carteret, M. J. Stébé, J. L. Blin, *J. Dispersion Sci. Technol.* **2011**, *32*, 1771–1779.

[6] C. Etrillard, V. Faramarzi, J. F. Dayen, J. F. Létard, B. Doudin, *Chem. Commun.* **2011**, *47*, 9663–9665.

[7] A. Rotaru, I. A. Gura'skiy, G. Molnár, L. Salmon, P. Demont, A. Bousseksou, *Chem. Commun.* **2012**, *48*, 4163–4165.

[8] P. Guionneau, M. Marchivie, G. Bravic, J.-F. Létard, D. Chasseau, *Top. Curr. Chem.* **2004**, *234*, 97; M. A. Halcrow, *Chem. Soc. Rev.* **2011**, *40*, 4119.

[9] A. Grosjean, N. Daro, B. Kauffmann, A. Kaiba, J. F. Létard, P. Guionneau, *Chem. Commun.* **2011**, *47*, 12382–12384.

[10] A. Grosjean, P. Guionneau, J. F. Létard, N. Daro, in preparation.

[11] C. Etrillard, PhD Thesis, University of Bordeaux, **2011**.

[12] A. Michalowicz, J. Moscovici, B. Ducourant, D. Cracco, O. Kahn, *Chem. Mater.* **1995**, *6*, 1404; M. Verelst, L. Sommier, P. Lecante, A. Mosset, O. Kahn, *Chem. Mater.* **1998**, *10*, 980.

[13] A. Urakawa, W. V. Beek, M. Monrabal-Capilla, J. R. Galan-Mascaros, L. Palin, M. Milanesio, *J. Phys. Chem. C* **2011**, *115*, 1323.

[14] S. J. J. Billinge, M. G. Kanatzidis, *Chem. Commun.* **2004**, 749.

[15] T. Forestier, A. Kaiba, S. Pechev, D. Denux, P. Guionneau, C. Etrillard, N. Daro, E. Freysz, J. F. Létard, *Chem. Eur. J.* **2009**, *15*, 6122–6130.

[16] T. Forestier, S. Mornet, N. Daro, T. Nishihara, S. Mouri, K. Tanaka, O. Fouche, E. Freysz, J. F. Létard, *Chem. Commun.* **2008**, 4327–4329.

[17] Materials Studio Modeling v. 5.5, detail information is available at http://accelrys.com/products/materials-studio.

[18] M. A. Neumann, *J. Appl. Crystallogr.* **2003**, *36*, 356–365.

[19] G. S. Pawley, *J. Appl. Crystallogr.* **1981**, *14*, 357–361.

[20] H. Toraya, F. Marumo, *Miner. J.* **1981**, *10*, 211–221.

[21] H. M. Rietveld, *J. Appl. Crystallogr.* **1969**, *2*, 65–71.

[22] X. Qiu, J. W. Thompson, S. J. L. Billinge, *J. Appl. Crystallogr.* **2004**, *37*, 678–678.

[23] C. L. Farrow, P. Juhás, J. W. Liu, D. Bryndin, E. S. Bozin, J. Bloch, Th. Proffen, S. J. L. Billinge, *J. Phys. Condens. Matter* **2007**, *19*, 335219.